Biosensors and Bioelectronics 65 (2015) 295–301

Contents lists available at ScienceDirect

Biosensors and Bioelectronics

journal homepage: www.elsevier.com/locate/bios

3D metal-organic framework as highly efficient biosensing platform for ultrasensitive and rapid detection of bisphenol A

Xue Wang [a,b], Xianbo Lu [a,*], Lidong Wu [c], Jiping Chen [a,*]

[a] Key Laboratory of Separation Science for Analytical Chemistry, Dalian Institute of Chemical Physics, Chinese Academy of Sciences, Dalian 116023, China
[b] University of Chinese Academy of Sciences, Beijing 100049, China
[c] Chinese Academy of Fishery Sciences, Beijing 100141, China

ARTICLE INFO

Article history:
Received 10 July 2014
Received in revised form
24 September 2014
Accepted 5 October 2014
Available online 14 October 2014

Keywords:
Metal-organic frameworks (MOFs)
Bisphenol A
Porous nanomaterials
Tyrosinase
Electrochemical biosensor

ABSTRACT

As is well known, bisphenol A (BPA), usually exists in daily plastic products, is one of the most important endocrine disrupting chemicals. In this work, copper-centered metal-organic framework (Cu-MOF) was synthesized, which was characterized by SEM, TEM, XRD, FTIR and electrochemical method. The resultant Cu-MOF was explored as a robust electrochemical biosensing platform by choosing tyrosinase (Tyr) as a model enzyme for ultrasensitive and rapid detection of BPA. The Cu-MOF provided a 3D structure with a large specific surface area, which was beneficial for enzyme and BPA absorption, and thus improved the sensitivity of the biosensor. Furthermore, Cu-MOF as a novel sorbent could increase the available BPA concentration to react with tyrosinase through π–π stacking interactions between BPA and Cu-MOF. The Tyr biosensor exhibited a high sensitivity of 0.2242 A M^{-1} for BPA, a wide linear range from 5.0×10^{-8} to $3.0 \times 10-6$ mol L^{-1}, and a low detection limit of 13 nmol L^{-1}. The response time for detection of BPA is less than 11 s. The proposed method was successfully applied to rapid and selective detection of BPA in plastic products with satisfactory results. The recoveries are in the range of 94.0–101.6% for practical applications. With those remarkable advantages, MOFs-based 3D structures show great prospect as robust biosensing platform for ultrasensitive and rapid detection of BPA.

1. Introduction

As one of the most important endocrine disrupting chemicals (EDCs), bisphenol A (BPA, 2.2-bis (4-hydroxyphenyl) propane) has received widespread attention. BPA can mimic the body's endogenous hormones by binding to estrogen receptors, which has been shown to adversely affect on endocrine system of human. In addition, BPA can also interfere with thyroid function, central nervous system, endocrine pancreas, immune system and reproduction system (Rochester, 2013). However, BPA is commonly used as a monomer in the synthesis of epoxy resins and polycarbonate plastics, such as feeding bottles, water bottles, food packaging, and cans (Schecter et al., 2010). Therefore, tremendous amount of BPA can migrate into food through leaching from final products, or into environment by wastewater discharge from plastic-producing industry. The US Environmental Protection Agency (EPA) reported that BPA was a high production volume chemical with a US volume estimated at 2.4 billion pounds in 2007, and releases of BPA to the environment exceeded one million pounds per year (US EPA, 2010). In China, there was a large BPA market, with an estimate of demand for BPA about 2.25 million tonnes in 2010 (Huang et al., 2012). European Union, China and the United States have banned BPA use in baby bottle and coating of infant formula packaging in recent years. Regarding high production volume, current pollution status and potential health risk of BPA, it is essential to develop a rapid, simple, sensitive and cost-effective method for determination of BPA.

Conventional analytical methods are available for determination of BPA, such as high performance liquid chromatography-fluorescence detector (HPLC-FLD) (Zhou et al., 2011), liquid chromatography-tandem mass spectrometry (LC-MS/MS) (Yazdinezhad et al., 2013), gas chromatography–mass spectrometry (GC–MS) (Lu et al., 2012). These techniques have advantages of high sensitivity and low detection limit. However, these methods require highly trained technicians, time-consuming sample preparations and expensive equipments. These limit the application of these methods in on-site monitoring or emergent detection. Hence, a number of innovative analytical methods were investigated in the past to overcome this hurdle. In recent years, electrochemical biosensors have attracted considerable attention for the advantages of low cost, fast response, simplified operation and inexpensive instrument. BPA is the substrate of tyrosinase. By using tyrosinase for the specifically catalytically oxidation of

* Corresponding authors. Fax: +86 411 84379562.
E-mail addresses: xianbolu@dicp.ac.cn (X. Lu), chenjp@dicp.ac.cn (J. Chen).

http://dx.doi.org/10.1016/j.bios.2014.10.010
0956-5663/

BPA, a few of electrochemical tyrosinase biosensors have been developed for determination of BPA, and some satisfactory results have been obtained (Ren et al., 2011; Wu et al., 2012a; Yin et al., 2010). The effective immobilization of enzyme molecules is one of the key factors in developing high performance enzyme biosensor. To seek for better immobilization matrixes, a variety of materials including graphene (Wang et al., 2010), mesoporous carbon (Wu et al., 2012b), metal nanoparticle (Saei et al., 2013), carbon nanotube (Vashist et al., 2011), metal oxide (Lu et al., 2008) and conducting polymer (Zhai et al., 2013) have already been explored to modify the electrodes for improving the loading amount as well as the bioactivity of the enzymes.

In the past decade, there is an explosive growth in the preparation, characterization, and study of materials known as metal-organic frameworks (MOFs) (Furukawa et al., 2013). MOFs are a new class of hybrid inorganic-organic porous crystalline materials with metal ions as the connectors and organic ligands as the linkers. MOFs have attracted considerable attention due to their extraordinarily high surface areas, tunable pore sizes, and adjustable internal surface properties (Zhou et al., 2012). Owing to these extraordinary properties, MOFs have been extensively applied for gas storage (Suh et al., 2012; Sumida et al., 2012), separation (Herm et al., 2014; Li et al., 2012), catalysis (Corma et al., 2010; Yoon et al., 2012), clean energy (Li and Xu, 2013), biomedicine (Horcajada et al., 2012) and chemical sensors (Kreno et al., 2012). According to our literature survey, there are only few preliminary attempts to incorporate and extend the functionality of MOFs as well as its derivatives into enzyme biosensor applications (Fu et al., 2011; Ma et al., 2013). Qin et al. reported that an amino-containing MOF (MIL-101(Al)–NH_2) was used to anchor hemin and the material showed peroxidase-like activity, which offered a colorimetric method for H_2O_2 determination. By coupling with glucose oxidase, a similar colorimetric method for analysis of glucose was also developed (Qin et al., 2013). Owing to the intrinsic limitations of biomimetic catalytic capability and indirect colorimetric method, the detection ability was not ideal compared to other electrochemical enzyme biosensors. If we can take advantage of the high biocatalytic activity of enzymes and the favorable microstructure and property of MOFs simultaneously, it will provide excellent opportunities for fabricating electrochemical enzyme biosensors based on MOFs with excellent performance.

Herein, we report an electrochemical tyrosinase biosensor for ultrasensitive detection of BPA. The Cu-MOF with a large surface area played an important role as the tyrosinase immobilization matrix. Additionally, the π–π stacking interactions between BPA and benzenedicarboxylate (BDC) ligands in Cu-MOF improved the pre-enrichment of BPA on the electrode surface, and thus increased the available concentration of enzyme substrates. The as-prepared Cu-MOF based biosensor exhibited excellent analytical performances with high sensitivity, fast response and low detection limit for determination of BPA in plastic products. The Cu-MOF based tyrosinase biosensor provides a promising method for the rapid and ultrasensitive detection of BPA.

2. Experimental

2.1. Reagents and chemicals

Triethylenediamine (TED), chitosan (from crab shells, minimum 85% deacetylated) and tyrosinase (from mushroom, >1000 units mg^{-1}) were purchased from Sigma-Aldrich (Shanghai, China). 1.4-benzendicarboxylic acid (1.4-H_2BDC) was purchased from Aladdin (Shanghai, China). Bisphenol A was obtained from Tokyo Chemical Industry Co. (Tokyo, Japan). All other reagents were of analytical grade and were used as received without further purification. 50 mmol L^{-1} phosphate buffer saline (PBS, pH 7.0) were prepared by mixing standard solutions of K_2HPO_4 and KH_2PO_4. Milli-Q water (18.2 MΩ cm) was used for the preparation of PBS.

2.2. Characterization of synthetic material

SEM images were recorded using a field emission scanning electron microscopy Supra 55 Sapphire (Zeiss, Germany) operated at 30 kV. TEM images were obtained using a transmission electron microscope Hitachi HT7700 (Hitachi, Japan) with an accelerating voltage of 120 kV. FTIR spectra was recorded by using a Spectrum GX (Perkin-Elmer, USA). The powder X-ray diffraction data were collected on a D/MAX2500PC X-ray diffractometer (Rigaku, Japan) with Cu Kα radiation ($\lambda=1.5418$ Å) over the 2θ range of 5°–50°. The scan step-width was set to 0.01° and the scan rate to 0.1° s^{-1} at room temperature. The XRD patterns were analyzed with MDI Jade 5.0 software (Materials Data Inc., USA). The N_2 gas adsorption-desorption was performed on an AutoSorb IQ2 micropore analyser (Quantachrome, USA). The cryogenic temperature was controlled using liquid nitrogen at 77 K. The outgassing process was carried out under vacuum at 373 K for 15 h.

2.3. Synthesis of Cu-MOF

The Cu-MOF was synthesized according to the previously reported method by Lee et al., 2007 with minor revision. Briefly, copper nitrate trihydrate (0.493 g), 1.4-H_2BDC (0.453 g) and TED (0.32 g) were dissolved in 100 mL DMF, and the mixture was sonicated to obtain a homogeneous solution. Then the solution was sealed in a 200 mL Teflon-lined autoclave and heated at 120 °C for 36 h. After slow cooling to room temperature, the obtained blue crystalline power was collected, washed with DMF several times and dried under vacuum overnight.

2.4. Preparation of the enzyme electrodes

Prior to modification, a glassy carbon electrode (GCE, 3 mm diameter) was polished carefully on a polishing cloth with 1.0, 0.3 and 0.05 μm alumina powder successively and rinsed with Milli-Q water followed by sonicating in ethanol and Milli-Q water. Then, the electrode was dried with purified nitrogen stream. To get the best performance of the biosensor, the composition of the CuMOF–Tyr–Chit was optimized. The final concentration of Cu-MOF, tyrosinase and chitosan was 0.5 mg mL^{-1}, 2.5 mg mL^{-1} and 1.5 mg mL^{-1}, respectively. The preparation process was as follows: Firstly, 10 μL tyrosinase solution (10 mg mL^{-1}) was added into 20 μL Cu-MOF suspension (1.0 mg mL^{-1}), and the mixture solution was shaked for 1 h. Then, 10 μL chitosan solution (6.0 mg mL^{-1}) were thoroughly mixed into the above solution. Finally, 4 μL of this mixture was cast onto the surface of a freshly polished GCE to prepare the CuMOF–Tyr–Chit/GCE biosensor, and then the electrode was dried at room temperature. When not in use, the fabricated electrode was stored in PBS at 4 °C in a refrigerator.

2.5. Electrochemical measurements

A CHI 440B Electrochemical Workstation (Chenhua Instruments, China) was used for cyclic voltammetry and amperometry. Cyclic voltammetric measurements were performed in pH 7.0 PBS at a scan rate of 100 mV s^{-1} ranging from +0.3 V to −0.5 V. Amperometric measurements were performed under an applied potential of −0.1 V. During the measurements, standard solution of BPA was added into 8 mL stirring pH 7.0 PBS at appropriate time intervals to obtain the corresponding signal.

Electrochemical impedance spectroscopy (EIS) measurements were carried out with a Metrohm Autolab PGSTAT302N Potentiostat/Galvanostat (Eco Chemie, The Netherlands). EIS measurements were

performed in 1 mmol L^{-1} $K_3[Fe(CN)_6]/K_4[Fe(CN)_6]$ (1:1) solution containing 0.5 mol L^{-1} KNO_3, with a frequency scan range from 1×10^5 to 1×10^{-1} Hz, and an amplitude of 10 mV. The results were plotted in the form of complex plane diagrams (Nyquist plots). All electrochemical measurements were carried out at room temperature with a conventional three-electrode system, where the prepared enzyme electrode was used as working electrode, an Ag/AgCl electrode (KCl concentration: 3 mol L^{-1}) as reference electrode, and a platinum wire as auxiliary electrode, respectively.

3. Results and discussion

3.1. Morphological and structural characterization of Cu-MOF

In this work, the Cu-MOF was synthesized using copper nitrate trihydrate, TED and 1.4-H_2BDC by a solvothermal method in DMF, according to a literature procedure with minor revision (Lee et al., 2007). The chemical structures of the secondary building units (SBU) in the assembled Cu-MOF are illustrated in Fig. 1A. Each paddle-wheel SBU is linked by BDC within the layer to form a 2D net parallel to the *xy* plane, which is further connected by TED molecules to produce a 3D framework. The crystal structure of pure Cu-MOF with permanent porosity and a large surface area is shown in Fig. 1B. The resultant Cu-MOF sample was then characterized by scanning electron microscopy (SEM), transmission electron microscopy (TEM), X-ray diffraction (XRD) and fourier transform infrared spectroscopy (FTIR).

The morphology, structure and size of the Cu-MOF samples were investigated by SEM and TEM. Fig. 1 clearly shows the synthesized Cu-MOF crystallites have a brick-like morphology. Higher magnification micrographs indicate that cubic shaped particles with an average crystal size of approximately 300 nm were obtained. Chitosan is a major constituent of the exoskeleton

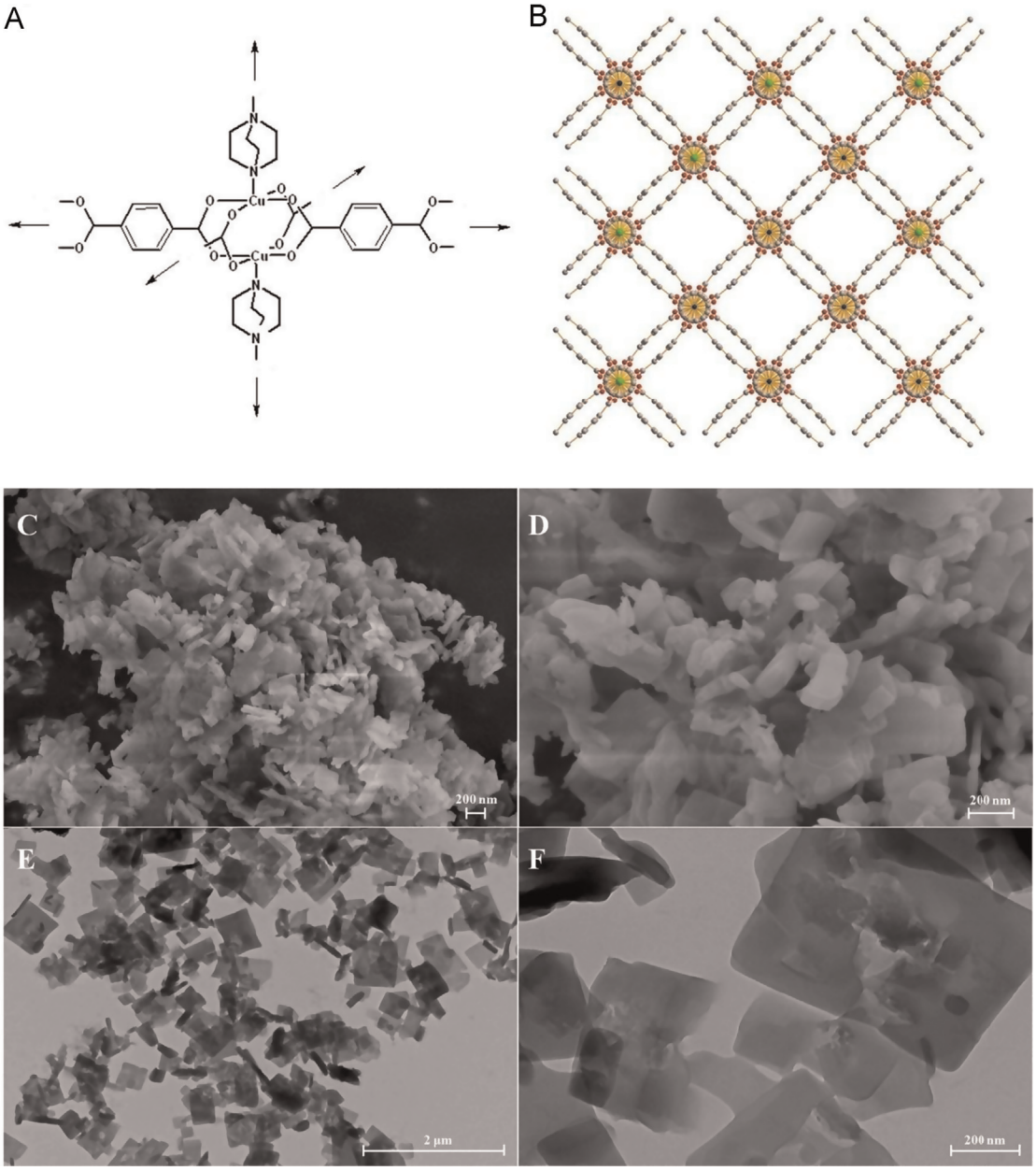

Fig. 1. (A) Chemical structure of the paddle wheel secondary building unit of Cu-MOF. (B) Crystal structure of Cu-MOF viewed along *c* axis. Cu (green), O (red), N (blue) and C (gray). For clarity, the H-atoms and solvent molecules are omitted. The morphology characteristics of Cu-MOF: (C, D) SEM images of Cu-MOF and (E, F) TEM images of Cu-MOF. (For interpretation of the references to color in this figure legend, the reader is referred to the web version of this article.)

material of crustaceans, cuttlefish and squid (Kurita, 2006). Due to its excellent biocompatibility, high permeability and film forming ability, chitosan has been extensively used for immobilization of enzymes and constructing electrochemical biosensors (Wu et al., 2012a; Zhang et al., 2014). In this work, a film layer was formed on the surface of electrode by dropping a mixture of Cu-MOF, tyrosinase and chitosan, as shown in Fig. S1 (Supporting Information). Swelling will happen after placing the film in aqueous media, which results in a porous structure of the film, and thus provide mass transfer channels for enzyme-catalyzed substrate and product. The rapid response time of the biosensor (11 s) further confirmed the rapid diffusion of enzyme–catalyzed substrate and product in the final porous film. Fig. S1B (Supporting Information) shows the cross-sectional view of the film and displays the final composite film has a porous structure. Fig. 2A provides the X-ray diffraction patterns of the Cu-MOF materials. A very sharp peak below 10° (with 2θ of 8.1°) is observed on the XRD diffractogram of the Cu-MOF, indicating that a highly crystalline material is achieved. Meanwhile, the intensive peaks appearing at small 2θ angles are also characteristics of porous materials which possesses numerous pores or cavities (Lin et al., 2011). The XRD pattern of as-prepared Cu-MOF has good agreement with the reported Cu-MOF in the literature, demonstrating that the Cu-MOF was successfully synthesized (Lee et al., 2007). The XRD pattern shows Cu-MOF is assigned to the tetragonal crystal system with unit cell parameter: $a=14.896$ Å, $c=19.159$ Å, space group: P4/ncc (No. 130). Additionally, the FTIR spectra for the functional groups in Cu-MOF are presented in Fig. 2B. There are strong peaks at 1389–1577 cm^{-1}, which is assigned to phenyl C=C ring stretch of the BDC linker. The peak at 1320 cm^{-1} is due to C–N stretching from TED (another ligand of the Cu-MOF). The peak at 567 cm^{-1} is due to Cu-O vibration, which is formed from the reaction of the BDC linker with the metal ion. Other fingerprint bands at 1623 cm^{-1}, 1055 cm^{-1} and 748 cm^{-1}, could be assigned to C=O vibration of COOH, C–O vibration and C–H benzene ring, respectively. Almost all the characteristic peaks of Cu-MOF can be found in the FTIR spectra, further indicating the Cu-MOF was obtained.

The pore structure was evaluated by nitrogen gas adsorption–desorption isotherm measured at 77 K. The diagram of Cu-MOF is illustrated in Fig. 2C, which reveals that Cu-MOF is microporous and exhibits typical type I reversible sorption profiles. The specific surface area was calculated in the relative pressure range from 0.001 to 0.026, and the results shows that the Brunauer–Emmett–Teller (BET) specific surface area of Cu-MOF is 1003 $m^2\,g^{-1}$. The Cu-MOF with a large specific surface area provides abundant binding sites for the immobilization of tyrosinase molecules, which is conducive to the sensitive detection of analytes. The

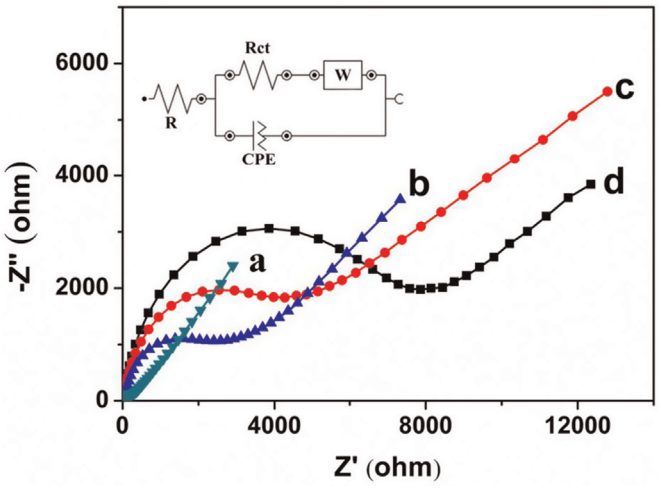

Fig. 3. Alternating-current impedance spectrums of bare GCE (a), Chit/GCE (b), CuMOF–Chit/GCE (c) and CuMOF–Tyr–Chit/GCE (d) in 1.0 mmol L^{-1} $Fe(CN)_6^{3-/4-}$ (1:1) containing 0.5 mol L^{-1} KNO_3 solution. The frequency range was from 1×10^5 to 1×10^{-1} Hz. Inset: Randles equivalent circuit used to fit the experiment data.

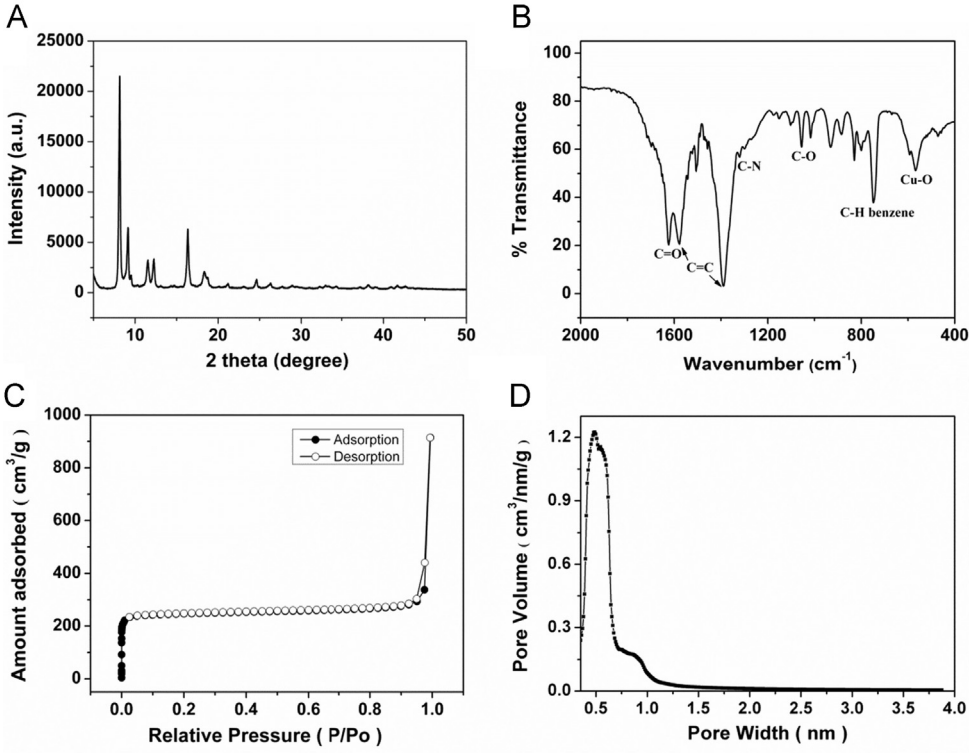

Fig. 2. (A) XRD pattern of Cu-MOF, (B) FTIR spectra of Cu-MOF, (C) adsorption-desorption isotherm of N_2 on Cu-MOF, and (D) the pore size distribution of Cu-MOF at 77 K.

Cu-MOF has a pore size distribution between 4 Å and 1.2 nm with a peak at ca. 4.9 Å, as calculated by the Saito-Foley method (Fig. 2D) (Song et al., 2011). The total volume calculated with nitrogen gas adsorbed at P/P_0 of 0.80 is 0.413 $cm^3\ g^{-1}$. In this work, Cu-MOF plays an important role for the immobilization of tyrosinase molecules and the larger surface is beneficial for enzyme absorption. Besides, the very large surface area of Cu-MOF is also beneficial for the π–π stacking interactions between BPA and Cu-MOF, which increase the available BPA concentration to react with tyrosinase.

3.2. Electrochemical characterization of CuMOF–Tyr–Chit/GCE

The electrochemical impedance spectroscopy (EIS) technique was utilized to characterize the interface properties of CuMOF–Tyr–Chit composite modified GCE. In the EIS, the semicircle portion observed at high frequencies corresponds to the electron transfer ability and the linear part at lower frequencies corresponds to the diffusion (Feng et al., 2005). The charge-transfer resistance (Rct) which controls the electron transfer kinetics of the redox probe at the electrode interface is gained by measuring the semicircle diameter. Fig. 3 displays the Nyquist plots of bare GCE (a), Chit/GCE (b), CuMOF-Chit/GCE (c) and CuMOF–Tyr–Chit/GCE (d) obtained in a 1.0 mmol L^{-1} $Fe(CN)_6^{3-/4-}$ (1:1) solution containing 0.5 mol L^{-1} KNO_3. The Randles equivalent circuit (Fig. 3, inset) was utilized to fit the experimental data, and the values of Rct for different electrodes were obtained in the following order: CuMOF–Tyr–Chit/GCE (7.11 kΩ) > CuMOF-Chit/GCE (4.54 kΩ) > Chit/GCE (2.65 kΩ) > bare GCE (0.26 kΩ). As can be observed, bare GCE presents a small semicircle domain, implying that it is almost a diffusion limiting process. After the modification of the electrode surface with a specific composite, the value of Rct changed, mainly caused by steric hindrance and electrostatic interactions (Bonanni et al., 2012). The Rct (2.65 kΩ) of Chit/GCE was much larger than that of the bare GCE (0.26 kΩ), indicating that a layer of chitosan had formed on the electrode surface. Even though chitosan can hinder the electron transfer from the redox probe of $[Fe(CN)_6]^{3-/4-}$ to the electrode surface, it is still widely used for constructing enzyme biosensors, because it can form an immobilized film with high mechanical strength and provide a biocompatible microenvironment for enzyme (Kang et al., 2009). With Cu-MOF immobilized on the chitosan film, the Rct increased from 2.65 kΩ to 4.54 kΩ. The Rct value of tyrosinase modified electrode further increased to 7.11 kΩ, indicated that tyrosinase had been successfully immobilized into the CuMOF-Chit film.

Previous study revealed that some Cu-based MOFs were electrochemically active because of the redox character of Cu^{2+} center (Mao et al., 2012). During redox process, the framework may tend to collapse and consequently resulting in the depression of the surface area and pore size of the MOFs. Fig. S2 (Supporting Information) shows the cyclic voltammogram of the CuMOF–Tyr–Chit/GCE in PBS at a scan rate of 100 mV s^{-1}. No redox peaks are observed on the CuMOF–Tyr–Chit/GCE, which reveals that Cu^{2+} center does not participate in the redox process, and thus Cu-MOF can maintain the original structure.

3.3. Bioelectrocatalytic activity of CuMOF–Tyr–Chit/GCE towards BPA

To evaluate the bioelectrocatalytic activity of CuMOF–Tyr–Chit/GCE, the modified electrode was characterized by cyclic voltammograms in the presence of BPA at the potential range between +0.3 and −0.5 V. In our study, 50 mmol L^{-1} pH 7.0 PBS was used as the electrolyte in electrochemical experiments because tyrosinase had the highest bioactivity in this pH value. Fig. S3 (Supporting Information) shows the cyclic voltammograms of the CuMOF-Tyr-Chit/GCE in 50 mM PBS (pH 7.0) in the presence of 3 μM BPA (curve a) and in the absence of BPA (curve b) at a scan rate of 100 mV s^{-1}. It was observed that with the addition of 3 μM BPA, both the oxidation current and reduction current increase. Obviously, the observed increase of redox current is attributed to the enzyme-catalyzed reaction on the electrode surface (Fig. S4, Supporting Information). The mechanism for the enzymatic reaction on the tyrosinase biosensor can be concisely expressed as Eqs. (1) and (2) (Andreescu and Sadik, 2004)

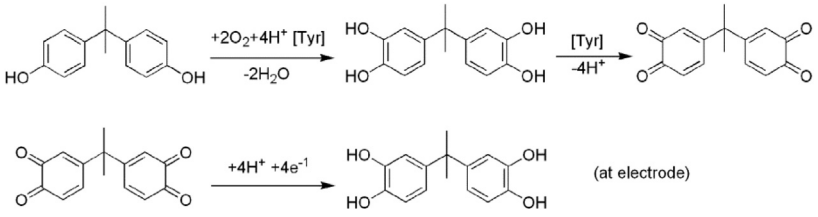

At a relatively low potential (−0.1 V peak potential), a large response toward BPA can be observed. It should be noted that relatively low applied potential is very important for tyrosinase biosensor as it reduces possible interferences in the detection. Thus, for further amperometric study of CuMOF–Tyr–Chit/GCE, a potential of −0.1 V (vs. Ag/AgCl: 3 M KCl) was applied.

3.4. Amperometric biosensing of BPA

Regarding the health risk of BPA, it is essential to develop a simple and rapid biosensing method for the detection of BPA. Fig. 4A illustrates and compares the amperometric responses (at −0.1 V) of CuMOF–Tyr–Chit/GCE (curve a), Tyr-Chit/GCE (curve b) and CuMOF–Chit/GCE (curve c) to the successive additions of BPA under constant stirring. The CuMOF–Chit/GCE without tyrosinase was completely unresponsive to the changes of BPA concentration. However, well-defined amperometric signals were observed for the BPA additions in the presence of tyrosinase on the Tyr–Chit/GCE and CuMOF–Tyr–Chit/GCE, reaching 95% of steady state current within 11 s. As shown in Fig. 4B, the CuMOF–Tyr–Chit/GCE exhibits substantially larger response signals than Tyr–Chit/GCE, indicating that the Cu-MOF with a large surface area could improve enzyme adsorption. In addition, Cu-MOF has a very large surface area (> 1000 $m^2\ g^{-1}$), and the surface of Cu-MOF is unable to be completely covered by enzyme molecules. Besides, according to the published references (e.g. Cui et al., 2009), the high affinity of the MOF-199 to benzene homologues results from the π–π interactions of the aromatic rings of the analytes with the framework 1.3.5-benzenetricarboxylic acid molecules. In another reference (Hu

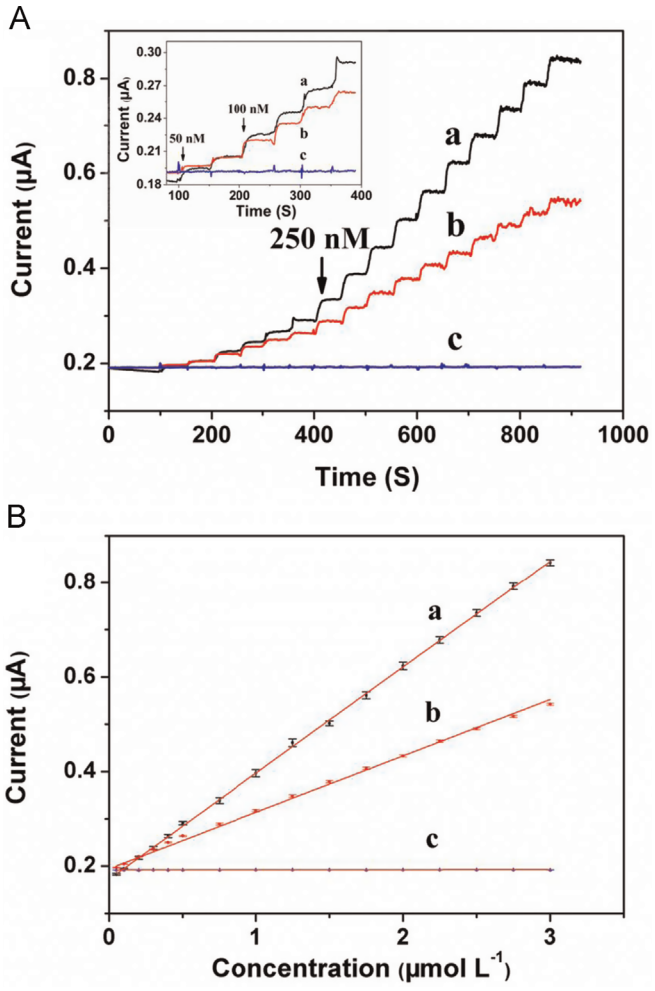

Fig. 4. (A) Amperometric current-time response curves of the CuMOF–Tyr–Chit/GCE (a), Tyr–Chit/GCE (b) and CuMOF–Chit/GCE (c) upon successive addition of BPA with different concentrations into a stirring solution 50 mM PBS (pH 7.0, 8 ml). Applied potential: −0.1 V versus Ag/AgCl. Inset: amplified response curve. (B) The linear calibration curve for BPA concentrations from 50 nM to 3 μM with a RSD of 7.0%.

et al., 2013), it reveals the polycyclic aromatic hydrocarbons allow π–π stacking interaction with the aromatic rings of terephthalic acid molecules in the framework of MOF-5. Based on the previously reported studies and the chemical structure of BPA and Cu-MOF, we suppose there may be π-π stacking interactions between BPA and Cu-MOF. BPA could be pre-enriched on the electrode surface to increase the local concentration of target analytes. The sensitivity of CuMOF–Tyr–Chit/GCE is 224.2 mA M^{-1}, which is about 2 times that of Tyr–Chit/GCE (116.5 mA M^{-1}). The linear range of the Cu-MOF based biosensor is from 5.0×10^{-8} to $3.0\times10-6$ mol L^{-1} with a correlation coefficient of 0.9998. The detection limit is estimated to be 13 nmol L^{-1} (signal-to-noise ratio, S/N=3). The analytical performances of the CuMOF–Tyr–Chit/GCE biosensor were compared with other enzyme biosensors that have been developed previously (Table 1). From Table 1, it can be seen that the sensitivity of the Cu-MOF based biosensor is higher than that of the graphene (Wu et al., 2012a), carbon nanotubes (Mita et al., 2007; Ren et al., 2011; Yin et al., 2010) or carbon-black (Portaccio et al., 2010; Portaccio et al., 2013) based biosensor. The Cu-MOF biosensor exhibits the lowest detection limit and the highest sensitivity for BPA among those biosensors. These results suggest that our developed biosensor is an excellent candidate for the ultrasensitive and rapid detection of BPA.

3.5. *Repeatability, reproducibility, stability and application to real sample analysis*

The repeatability of the CuMOF–Tyr–Chit/GCE biosensor was investigated by the detection of 0.25 μM BPA. A relative standard deviation (RSD) value of 7.3% was obtained for 8 successive determinations, indicating acceptable repeatability of the method. Similarly, the electrode-to-electrode fabrication reproducibility was also estimated by determining the response of 0.25 μM BPA at five individual electrodes, and the RSD was 10.3%, revealing the method had acceptable reproducibility. The enzyme electrode was stored in PBS (50 mM, pH 7.0) at 4 °C in a refrigerator. The storage stability of the biosensor was evaluated by detecting the amperometric response to 0.25 μM BPA. The results showed that the biosensor retained 90% of its original response after 3 weeks, demonstrating its good long-term stability.

In order to evaluate the performance of CuMOF–Tyr–Chit/GCE biosensor for real sample analysis, the biosensor was used to detect BPA leaching from plastic samples. In brief, different kinds of commercial plastic products (purchased from a local supermarket) were cut into small pieces and washed thoroughly with Milli-Q water. Then 1.0 g of plastic product pieces and 30 mL water were added into to a conical flask, which was sealed and heated at 70 °C for 48 h. After filtrated, the liquid phase was collected in a 50 mL volumetric flask and diluted to 50 mL with Milli-Q water. A known-amount of the obtained sample solution was analyzed by the biosensor with amperometric measurement. The obtained results are shown in Table 2. The content of the BPA in water bottle (PC) sample was calculated to be 6.2 μg/g. BPA was not detectable in the other plastic samples such as nursing bottle (PP), coffee spoon (PP) and mineral water bottle (PET). The recoveries of BPA standard solution added into the plastic samples were in the range of 94.0–101.6%.

BPA is usually used as a plasticizer for the production of PC. Because some chemical bonds in PC are unstable, BPA can leach into water when the PC products are filled with water. The good selectivity of the biosensor is attributed to the biocatalytic specificity of tyrosinase for BPA. Other potential co-existing plasticizer

Table 1
Comparison of analytical performances of the CuMOF-Tyr-Chit/GCE biosensor with other enzyme biosensors for detection of BPA.

Modified electrode[a]	Linear range (μM)	Sensitivity (A M^{-1})	Detection limit (nM)	Reference
CuMOF–Tyr–Chit/GCE	0.05–3	0.2242	13	This paper
NGP–Tyr–Chit/GCE	0.1–2	0.2196	33	Wu et al. (2012a)
MWNTs-Tyr/GCE	2–100	–	500	Ren et al. (2011)
MWNTs–Tyr–SF–CoPc/GCE	0.05–3	–	30	Yin et al. (2010)
Thionine–Tyr/CPE	0.15–45	0.0854	150	Portaccio et al. (2010)
SWCN–Tyr–mineral oil/CPE	0.1–12	0.138	20	Mita et al. (2007)
Thionine–laccase–carbon black/SPE	0.5–50	0.005	200	Portaccio et al. (2013)

[a] NGP=hydrophilic nanographene, MWNTs=multiwall carbon nanotubes, SF=silk fibroin, CoPc=cobalt phthalocyanine, CPE=carbon paste electrode, SWCN=single wall carbon nanotubes, SPE=screen printed electrode.

Table 2
Determination of BPA in plastic samples.

Sample[a]	Measured (μM)[b]	Added (μM)	Found (μM)[b]	Recovery (%)
Water bottle (PC)	0.543	0.5	1.017	97.5
Nursing bottle (PP)	n.d.[c]	0.5	0.508	101.6
Coffee spoon (PP)	n.d.	0.5	0.470	94.0
Mineral water bottle (PET)	n.d.	0.5	0.494	98.8

[a] PC=polycarbonate; PP=polypropylene; PET=polyethylene terephthalate.
[b] The average value of three determinations.
[c] n.d. means "not detectable".

interferences (e.g. phthalates) are not the substrate of tyrosinase, which will not interfere with the detection of BPA by tyrosinase based biosensors (Wu et al., 2012a). In addition, common inorganic ions (such as 2 mM K^+, Na^+, NO_3^-, $H_2PO_4^-$, HPO_4^{2-}, Cl^- and Ac^-) and organic solvents (such as 0.25% v/v acetone, acetonitrile, methanol and ethanol) have no influence on the performance of the biosensor. Some phenolic chemicals (e.g. phenol and catechol) were not used as monomers and additives in the production of PC products (Yang et al., 2011). Therefore, these phenolic chemicals have no effect on the specific usage of the biosensor for the detection of BPA leaching from PC products.

4. Conclusion

In this study, we have developed a novel Cu-MOF based biosensing platform for ultrasensitive and rapid detection of BPA. The higher sensitivity of the Cu-MOF based biosensor might be due to the concentration effect of BPA in the enzyme film, which increase the available BPA concentration to react with tyrosinase, because of the π–π stacking interactions between BPA and Cu-MOF. The very large surface area of Cu-MOF is beneficial for the π–π stacking interactions and enzyme absorption. The proposed method was successfully applied to determine BPA in plastic products with satisfactory results. The Cu-MOF based tyrosinase biosensor provides a simple, rapid, cost-effective and ultrasensitive method for the detection of BPA in plastic products. By using other biomolecules as recognition elements, the developed Cu-MOF biosensing platform could be extended toward the rapid detection of other targets.

Acknowledgments

This work was supported by the National High Technology Research and Development Program of China (No. 2013AA065203), the National Natural Science Foundation of China (No. 20907051), and the Youth Innovation Promotion Association, CAS (No. 2060303).

Appendix A. Suplementary material

Supplementary data associated with this article can be found in the online version at 10.1016/j.bios.2014.10.010.

References

Andreescu, S., Sadik, O.A., 2004. Anal. Chem. 76, 552–560.
Bonanni, A., Loo, A.H., Pumera, M., 2012. Trac-Trends Anal. Chem. 37, 12–21.
Corma, A., Garcia, H., Xamena, F.X.L.I., 2010. Chem. Rev. 110, 4606–4655.
Cui, X.Y., Gu, Z.Y., Jiang, D.Q., Li, Y., Wang, H.F., Yan, X.P., 2009. Anal. Chem. 81, 9771–9777.
Feng, J.J., Zhao, G., Xu, J.J., Chen, H.Y., 2005. Anal. Biochem. 342, 280–286.
Fu, Y.C., Li, P.H., Bu, L.J., Wang, T., Xie, Q.J., Chen, J.H., Yao, S.Z., 2011. Anal. Chem. 83, 6511–6517.
Furukawa, H., Cordova, K.E., O'Keeffe, M., Yaghi, O.M., 2013. Science 341974.
Herm, Z.R., Bloch, E.D., Long, J.R., 2014. Chem. Mater. 26, 323–338.
Horcajada, P., Gref, R., Baati, T., Allan, P.K., Maurin, G., Couvreur, P., Ferey, G., Morris, R.E., Serre, C., 2012. Chem. Rev. 112, 1232–1268.
Hu, Y.L., Huang, Z.L., Liao, J., Li, G.K., 2013. Anal. Chem. 85, 6885–6893.
Huang, Y.Q., Wong, C.K.C., Zheng, J.S., Bouwman, H., Barra, R., Wahlstrom, B., Neretin, L., Wong, M.H., 2012. Environ. Int. 42, 91–99.
Kang, X.H., Wang, J., Wu, H., Aksay, I.A., Liu, J., Lin, Y.H., 2009. Biosens. Bioelectron. 25, 901–905.
Kreno, L.E., Leong, K., Farha, O.K., Allendorf, M., Van Duyne, R.P., Hupp, J.T., 2012. Chem. Rev. 112, 1105–1125.
Kurita, K., 2006. Mar. Biotechnol. 8, 203–226.
Lee, J.Y., Olson, D.H., Pan, L., Emge, T.J., Li, J., 2007. Adv. Funct. Mater. 17, 1255–1262.
Li, J.R., Sculley, J., Zhou, H.C., 2012. Chem. Rev. 112, 869–932.
Li, S.L., Xu, Q., 2013. Energy Environ. Sci. 6, 1656–1683.
Lin, K.S., Adhikari, A.K., Chang, K.C., Tu, M.T., Lu, W., 2011. Catal. Today 164, 23–27.
Lu, J., Wu, J., Stoffella, P.J., Wilson, P.C., 2012. J. Chromatogr. A 1258, 128–135.
Lu, X.B., Zhang, H.J., Ni, Y.W., Zhang, Q., Chen, J.P., 2008. Biosens. Bioelectron. 24, 93–98.
Ma, W.J., Jiang, Q., Yu, P., Yang, L.F., Mao, L.Q., 2013. Anal. Chem. 85, 7550–7557.
Mao, J.J., Yang, L.F., Yu, P., Wei, X.W., Mao, L.Q., 2012. Electrochem. Commun. 19, 29–31.
Mita, D.G., Attanasio, A., Arduini, F., Diano, N., Grano, V., Bencivenga, U., Rossi, S., Amine, A., Moscone, D., 2007. Biosens. Bioelectron. 23, 60–65.
Portaccio, M., Di Tuoro, D., Arduini, F., Lepore, M., Mita, D.G., Diano, N., Mita, L., Moscone, D., 2010. Biosens. Bioelectron. 25, 2003–2008.
Portaccio, M., Di Tuoro, D., Arduini, F., Moscone, D., Cammarota, M., Mita, D.G., Lepore, M., 2013. Electrochim. Acta 109, 340–347.
Qin, F.X., Jia, S.Y., Wang, F.F., Wu, S.H., Song, J., Liu, Y., 2013. Catal. Sci. Technol 3, 2761–2768.
Ren, J., Kang, T.F., Xue, R., Ge, C.N., Cheng, S.Y., 2011. Microchim. Acta 174, 303–309.
Rochester, J.R., 2013. Reprod. Toxicol. 42, 132–155.
Saei, A.A., Najafi-Marandi, P., Abhari, A., de la Guardia, M., Dolatabadi, J.E.N., 2013. Trac-Trends Anal. Chem. 42, 216–227.
Schecter, A., Malik, N., Haffner, D., Smith, S., Harris, T.R., Paepke, O., Birnbaum, L., 2010. Environ. Sci. Technol. 44, 9425–9430.
Song, P., Li, Y.Q., Li, W., He, B., Yang, J.Z., Li, X.G., 2011. Int. J. Hydrog. Energy 36, 10468–10473.
Suh, M.P., Park, H.J., Prasad, T.K., Lim, D.W., 2012. Chem. Rev. 112, 782–835.
Sumida, K., Rogow, D.L., Mason, J.A., McDonald, T.M., Bloch, E.D., Herm, Z.R., Bae, T. H., Long, J.R., 2012. Chem. Rev. 112, 724–781.
US. EPA, 2010. Bisphenol A Action Plan.
Vashist, S.K., Zheng, D., Al-Rubeaan, K., Luong, J.H.T., Sheu, F.S., 2011. Biotechnol. Adv. 29, 169–188.
Wang, Y., Shao, Y.Y., Matson, D.W., Li, J.H., Lin, Y.H., 2010. ACS Nano 4, 1790–1798.
Wu, L.D., Deng, D.H., Jin, J., Lu, X.B., Chen, J.P., 2012a. Biosens. Bioelectron. 35, 193–199.
Wu, L.D., Lu, X.B., Zhang, H.J., Chen, J.P., 2012b. ChemSusChem 5, 1918–1925.
Yang, C.Z., Yaniger, S.I., Jordan, V.C., Klein, D.J., Bittner, G.D., 2011. Environ. Health Perspect. 119, 989–996.
Yazdinezhad, S.R., Ballesteros-Gomez, A., Lunar, L., Rubio, S., 2013. Anal. Chim. Acta 778, 31–37.
Yin, H.S., Zhou, Y.L., Xu, J., Ai, S.Y., Cui, L., Zhu, L.S., 2010. Anal. Chim. Acta 659, 144–150.
Yoon, M., Srirambalaji, R., Kim, K., 2012. Chem. Rev. 112, 1196–1231.
Zhai, D.Y., Liu, B.R., Shi, Y., Pan, L.J., Wang, Y.Q., Li, W.B., Zhang, R., Yu, G.H., 2013. ACS Nano 7, 3540–3546.
Zhang, Y.W., Li, Y.Q., Wu, W.J., Jiang, Y.R., Hu, B.R., 2014. Biosens. Bioelectron. 60, 271–276.
Zhou, H.C., Long, J.R., Yaghi, O.M., 2012. Chem. Rev. 112, 673–674.
Zhou, Q.X., Gao, Y.Y., Xie, G.H., 2011. Talanta 85, 1598–1602.